Letter

High-Performance Cryogen-Free Platform for Microkelvin-Range Refrigeration

J. Nyéki,[1] M. Lucas,[1] P. Knappová,[1] L.V. Levitin,[1] A. Casey,[1,*] J. Saunders,[1] H. van der Vliet,[2] and A.J. Matthews[2]

[1] *Department of Physics, Royal Holloway, University of London, Egham, Surrey TW20 0EX, United Kingdom*
[2] *Oxford Instruments NanoScience, Tubney Woods, Abingdon, Oxfordshire OX13 5QX, United Kingdom*

(Received 12 April 2022; revised 25 July 2022; accepted 12 September 2022; published 24 October 2022)

Improved accessibility to the microkelvin temperature regime is important for future research in quantum materials, for quantum information science, and for applications of quantum sensors. Here, we report the design and performance of a microkelvin platform based on a nuclear-demagnetization stage, engineered and well optimized for operation on a standard cryogen-free dilution refrigerator. $PrNi_5$ is used as the dominant refrigerant. The platform provides a large area for mounting experiments in an ultralow-temperature low-electromagnetic-noise environment. The performance is characterized using current-sensing noise thermometry. Temperatures as low as 395 μK are reached and a protocol is established in which it is possible to operate experiments below 1 mK for 95% of the time, providing an efficient cryogen-free microkelvin environment for a wide range of science applications.

DOI: 10.1103/PhysRevApplied.18.L041002

Background.—Advances in cryogen-free dilution refrigeration [1,2] have played a crucial role in the development of superconducting quantum technology for computing and sensing. The microkelvin temperature regime represents a strategically important frontier for quantum information science. Cryogen-free technology is essential to promote the accessibility of this regime and to ensure sustainability, beyond specialist infrastructures such as the European Microkelvin Platform [3]. Cooling into this regime is achieved by adiabatic nuclear demagnetization [4]. The nuclear spins of a suitable material are polarized in an external magnetic field and cooled to dilution-refrigerator temperatures. After thermally isolating the material, the external field is then reduced. Under approaching isentropic conditions, in the absence of interactions, $T_f = T_i B_f / B_i$, where T_i and T_f refer to the initial and final temperature, and B_i and B_f are the corresponding initial and final magnetic field.

The range of quantum materials and quantum sensors of interest for quantum information science is extremely diverse. Access to lower temperatures will yield fundamental insights into two-level fluctuators in superconducting qubits [5,6], which are a barrier to fault-tolerant quantum computing [7,8]. Further cooling of two-dimensional electron gases [9] will promote understanding of aspects of the fractional quantum Hall effect [10] and drive the development of semiconductor devices, including spintronic devices [11,12]. There is an ongoing search for a crystalline topological superconductor [13–18] and $YbRh_2Si_2$ [19] is a candidate material that requires temperatures below a few millikelvins. When cooling below 2.5 mK, ^{3}He provides a benchmark for topological superconductivity, displaying a wealth of phenomena in the surface and edge states that arise from bulk-surface correspondence [20–23]. Strongly correlated electron systems exhibit quantum criticality [24–26], which is essentially a $T = 0$ phenomenon. An exciting direction is the extension of studies of quantum criticality to lower temperature; for example, to understand the role of nuclear magnetism, particularly in systems with strong hyperfine interactions [27–30]. Cooling to below 1 mK allows access to magnetic field-to-temperature ratios, B/T, that are unachievable elsewhere. High B/T ratios are of particular interest in heavy fermion systems and also to investigate hyperfine effects. Finally, microkelvin platforms will be of increasing importance for hosting quantum sensors for fundamental physics, such as dark-matter searches and quantum simulators. These may require locating in underground facilities, where cryogen-free operation is optimal.

Significant effort has been devoted to on-chip cooling technologies [31,32]. Two successful approaches to reaching microkelvin temperatures have been either by parallel nuclear demagnetization of each lead connected to a sample [33,34] or by the incorporation of nuclear refrigeration elements directly on-chip, where the device is itself a thermometer (a Coulomb-blockade thermometer), which directly measures the electron temperature [35,36].

*a.casey@rhul.ac.uk, author to whom correspondence should be addressed

Our approach is to treat the cooling of the microkelvin platform and the thermalization of the device or sample to this platform separately. The merit of this approach is its flexibility and applicability to a wide range of materials and devices. On traditional "wet cryostats," we have demonstrated cooling of a two-dimensional electron gas below 1 mK in a ^{3}He immersion cell [37], thermodynamic and transport measurements on a heavy fermion superconductor $YbRh_2Si_2$ down to 200 μK [38], and an ac susceptibility study of superconductivity and antiferroquadrupole order in $PrOs_4Sb_{12}$ [39] down to 1 mK, reaching a B/T value in excess of 6000 T/K. In combination with cryogen-free operation, this opens up a wide landscape for research on quantum materials into the microkelvin regime.

Introduction.—A *proof-of-principle* cryogen-free nuclear-demagnetization platform [40] has been based upon a $PrNi_5$ nuclear stage, that had been originally constructed for a traditional "wet system" [41]. This demonstrated that the vibrations inherent in a pulse-tube-cooled cryostat [42] are not incompatible with nuclear demagnetization. Cryogen-free systems with copper nuclear-demagnetization stages have been developed reaching temperatures below 100 μK [34,43,44]. Designs of continuous cryogen-free nuclear-demagnetization systems have been proposed [45,46] but have yet to demonstrate their performance.

The focus of this letter is a cryogen-free microkelvin platform capable of achieving temperatures below 500 μK, with a hold time below 1 mK, suitable for the applications discussed previously. A rapid thermal turnaround time dramatically enhances the efficiency of an experiment, with a greater fraction of time being spent in the temperature range of interest. A key figure of merit is the thermal "duty cycle," which we define as the percentage of the total time of the single-shot cooling cycle spent below 1 mK. For our design, the best value achieved so far is 95%, a dramatic improvement over the previous published results for cryogen-free systems, ranging from 50% down to $< 10\%$ [40,43,44].

To achieve this result, we combine the favorable properties of the Van Vleck paramagnetic material $PrNi_5$, which has previously been used in traditional "wet cryostats" [4,47–51], with a well-designed thermal link, heat switch, and system to minimize the relative motion between the demagnetization magnet and the nuclear stage.

Essential to the characterization of the performance of the system is reliable thermometry. We adopt current-sensing noise thermometry (CSNT) [52,53], which can be used over the full temperature range.

Design details.—The design principle is for a system that will be compatible with a minimally modified cryogen-free dilution refrigerator, boosting the lowest temperatures that can be reached to below 500 μK (in this case, an Oxford Instruments Triton 200 [54]). The system is equipped with a 6-T superconducting magnet. Field compensation results in less than 10 mT in the ultralow-temperature (ULT) experimental region, when the magnet is at the full field. We adopt a modular design in which the thermal links interconnecting the main components of the platform use demountable cone joints [55].

A schematic of the system is shown in Fig. 1. All of the copper used in the construction is commercial OFE-OK copper [56]. Through heat treatment, the residual resistivity ratio (RRR) of the copper can be increased up to 3000. The mixing-chamber (MC) plate, the heat-switch (HS) plate, and the ULT plate are gold plated to prevent oxidization of the surfaces [57]. Each plate is equipped with a four-wire resistive heater for characterization. Simplicity and reproducibility of construction and the avoidance of hazardous materials and toxic chemicals in the construction process are also design criteria.

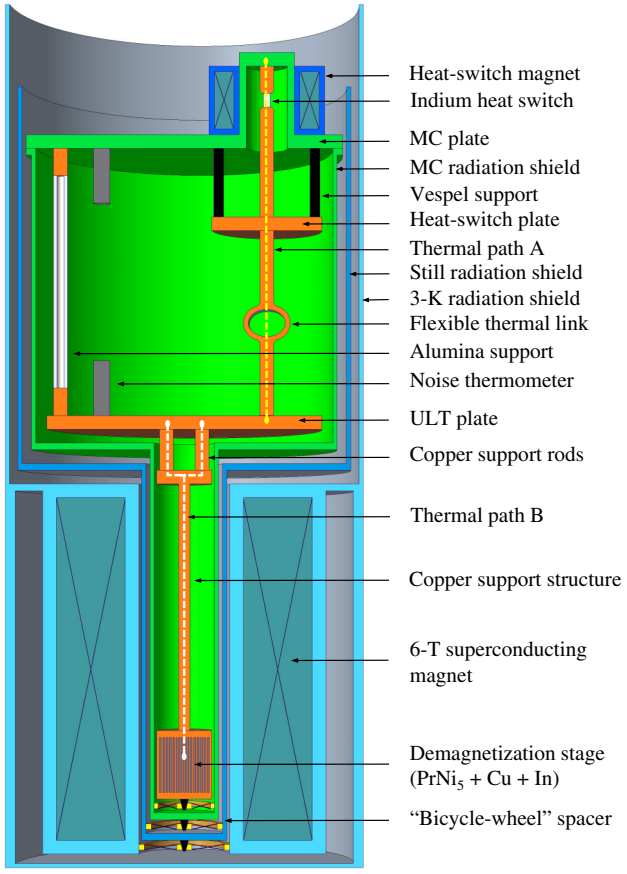

FIG. 1. A schematic diagram of the microkelvin platform. Enclosed in green is the ultralow-temperature low-electrical-noise region. The current-sensing noise thermometers on the ULT and MC plates are shown in gray. The thermal pathways for the link from the mixing chamber to the ULT plate and for the ULT plate to the $PrNi_5$ are marked by dashed lines.

The original cryostat MC plate is replaced by a design to meet the requirement for an rf-tight space for the microkelvin platform. The MC shield and plate enclose a large volume, creating an electrically quiet environment for measurements while reducing the heat leak to the ULT region. The HS magnet is mounted on the MC plate, outside of the rf shield. A CSNT (sensor resistance 300 mΩ) is mounted on the MC plate.

The experimental volume contains a relatively large area ULT plate, of diameter 240 mm, with a RRR of 265. The ULT plate is equipped with multiple mounting points for experiments, consisting of 14 cone joints, three of which have line-of-sight access to the room-temperature ports on the top of the cryostat. The ULT plate is suspended from the MC plate via alumina tubes. The thermal pathway to the MC plate is via a flexible copper link (annealed to achieve a RRR of 3000), the HS plate, and the robust indium heat switch. The HS plate is suspended from the MC plate using Vespel rods. A CSNT (sensor resistance 2 mΩ) is mounted on the ULT plate and is used to characterize the performance of the demagnetization process.

The nuclear-demagnetization stage is constructed out of polycrystalline $PrNi_5$ [58] of total mass 94.5 g (0.22 mole), supplied in the form of irregular rods, soldered using indium to a rigid copper support structure. The copper support structure (RRR of 1660) is attached to the ULT plate by copper rods with cone joints at each end. While all of the construction materials contribute to nuclear cooling, the dominant contribution arises from the $PrNi_5$. Hyperfine enhancement boosts the field seen by the ^{141}Pr nuclei by a factor of 11.2 above the externally applied field [59]. In 6 T, a significant entropy reduction ($> 80\%$) of the $PrNi_5$ can be achieved in the modest temperature range of 10–20 mK.

The small Korringa constant of praseodymium [60], κ, results in a negligible thermal resistance between the electrons and the nuclear spin system ($\kappa_{Pr} \sim 3$ μKs [61], compared to $\kappa_{Cu} = 1.2$ Ks for copper [4]). The thermal conductivity of polycrystalline $PrNi_5$ is poor, comparable to that of brass. The $PrNi_5$ rods have a RRR that varies from 7 to 30. It is therefore critical to optimize the heat transfer between the copper support structure and the $PrNi_5$. This is achieved using indium as a solder [51]. Cadmium has traditionally been used for this purpose [48] but has higher toxicity; zinc has recently been proposed [62] as an alternative material. Although indium limits the final field to be in excess of 28 mT, the superconducting critical field of indium, it does not compromise the achievement of the performance objectives.

To achieve a short precooling time, the thermal link between the MC plate and the nuclear stage is designed to be dominant relative to the cooling power of the MC. For comparison at the end of the precool shown in Fig. 2, the cooling power of the dilution refrigerator is $\dot{Q} = 5$ μ W, resulting in $\dot{Q}/T^2 \sim 12.2$ mW/K^2, less than half of the value $L/2R = 27$ mW/K^2 due to the thermal link, where L is the Lorenz number [63] and $R \sim 450$ nΩ is the total resistance between the $PrNi_5$ and the MC. Figure 1 shows this thermal pathway in two sections, *path A*, between the MC and ULT plate, and *path B*, between the ULT plate and the Pr nuclear spin bath. The measured thermal resistance of *path A*, with the heat switch in its normal state, corresponds, via the Weidemann-Franz law [64], to an electrical resistance of 300 nΩ. The superconducting heat switch assembly including cone joints contributes 170 nΩ to this value. The thermal conductivity of the open switch, measured at 100 mK, is 3×10^{-5} W cm^{-1}K^{-1}, equivalent to that achieved in aluminum heat switches [4,65]. The thermal resistance of *path B* is measured directly by applying heat to the ULT plate and corresponds to an electrical resistance of 150 nΩ.

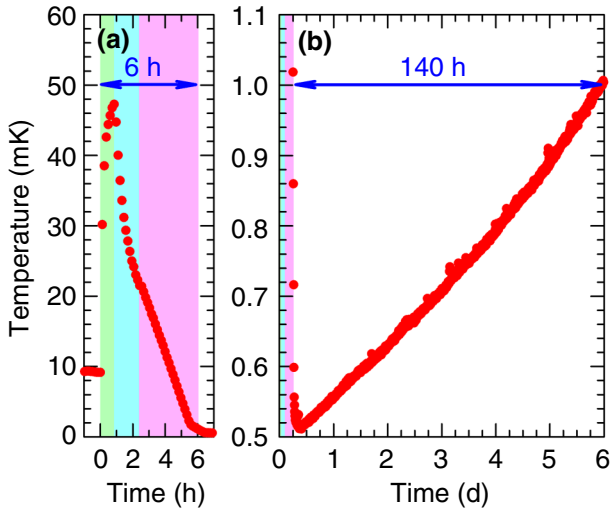

FIG. 2. (a) The preparation time for a "lunchtime" precool; the external magnetic field is ramped up to 6 T (green); the magnet is persisted and the nuclear stage is allowed to precool (blue); the heat switch is opened and the nuclear stage is demagnetized to 30 mT (pink). (b) The temperature of the ULT plate CSNT as a function of time following the demagnetization, showing a hold time of 140 h below 1 mK.

Key to the cooling performance achieved is the immunity to mechanical vibrations. It is most important to limit relative motion of the nuclear stage and the 6-T magnet. This is achieved by three similar "bicycle-wheel" spacers: between the stage and the MC shield; between the MC shield and the still shield; and between the still shield and main magnet (see Figs. 1 and 5, inset).

Performance.—To illustrate the duty cycle, we show in Fig. 2 a process in which the system starts in a low field at 9 mK; it is then magnetized to 6 T, followed by a rapid precool period of about 2 h. We refer to this as a "lunchtime" precool. After opening the superconducting heat switch, a demagnetization to a final field of 30 mT at a constant rate

of 1.75 T/h gives a final temperature around 500 μK. The heat leak due to eddy currents is measured to be 30 nW in the field interval from 5.6 T to 4.5 T. The platform remains below 1 mK for almost 6 d. With a longer precool time (15 h, referred to as an "overnight" precool), the starting temperature of the demagnetization is typically 10 mK and with a staggered demagnetization rate over a period of 7.5 h, a temperature of 395 μK is achieved. Eddy current heating in the copper structure, arising from vibrations while precooling in the high magnetic field and sweeping of the field during demagnetization, is tolerable despite its geometry and high RRR. Here, we exploit the high magnetoresistance of copper [66,67]; with RRR = 1660, the electrical resistance increases by a factor of over 20 in 6 T.

To quantify the heat leak and its field dependence, the total heat capacity of the nuclear stage is measured using the CSNT and a heater on the ULT plate. We exploit the achievable precision in short measurement times, t_m, using two-stage superconducting quantum interference device (SQUID) detection [68]. The noise floor of these devices allows the sensor resistor to range from a few mΩ to a few hundred mΩ and still have a reasonable noise temperature (in the range 5–100 μK). The 2-mΩ sensor of the CSNT delivers 1% precision in $t_m = 10$ s [52].

A typical heat pulse is shown in Fig. 3. The total stage heat capacity measured in this way for various magnetic fields is shown in Fig. 4. The residual heat leak in different magnetic fields is determined by simply observing the warm-up rate (see Fig. 5). We note that with this level of heat leak in low fields and the experimentally determined thermal resistance between the ULT plate and the $PrNi_5$, we can be confident that the CSNT is in good equilibrium with the stage. Thermalization of the CSNT to the ULT plate relies on filtering the leads between the SQUID and the sensor resistor [69].

The 4-nW field-independent heat leak at low fields Fig. 5 is subsequently reduced to 2 nW, by improvements in electrical and mechanical grounding of room-temperature services. The warm-up data in Fig. 2 are determined under

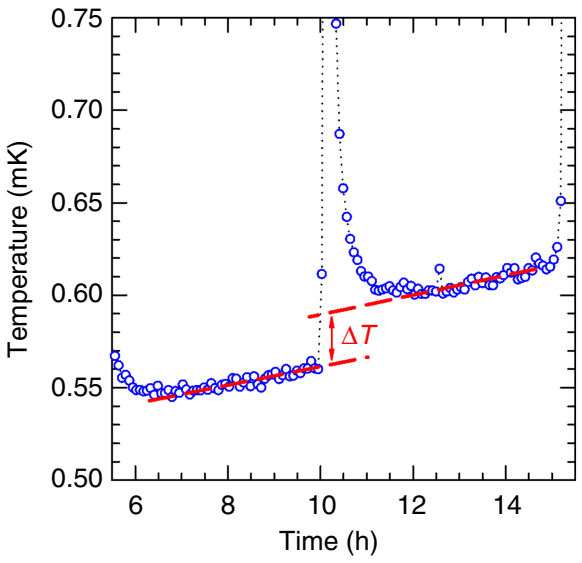

FIG. 3. A typical heat-pulse measurement to evaluate the heat capacity (approximately 70 nW applied for 10 min), demonstrating that a ΔT corresponding to a 5% temperature step can easily be resolved at temperatures as low as 0.5 mK.

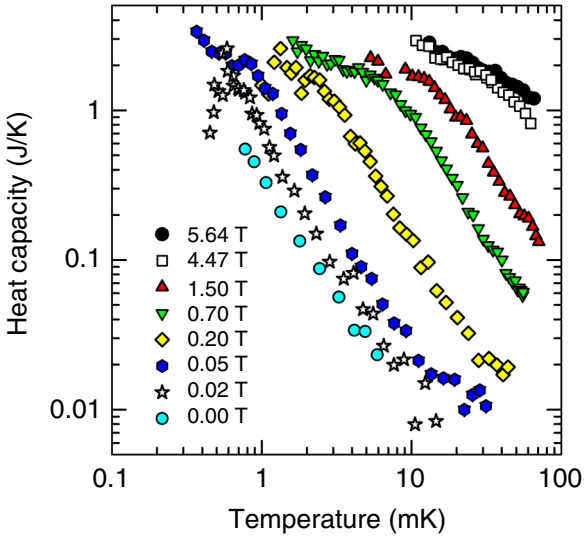

FIG. 4. The total heat capacity of the nuclear stage as a function of the temperature and the applied magnetic field, with $PrNi_5$ providing the dominant contribution.

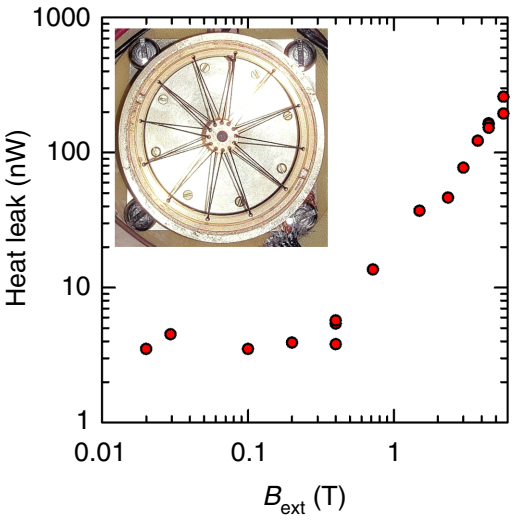

FIG. 5. The heat leak to the nuclear-demagnetization stage as a function of the external magnetic field, extracted from the warming data. Subsequent improvements result in a 30-mT heat leak of 2 nW, which is the heat leak under which the warming data shown in Fig. 2 are obtained. The inset shows the "bicycle-wheel" components connecting the still shield to the magnet.

these conditions and we estimate that the "overnight" precool will result in 2 weeks below 1 mK with such a low heat leak.

Conclusions.—We demonstrate the performance of a microkelvin platform that is modular, robust, and tolerant to mechanical vibrations. The platform can rapidly reach temperatures as low as 395 μK. The hold time below 1 mK represents an excellent duty cycle of 95%.

The platform provides a large electrically quiet experimental microkelvin volume, capable of hosting multiple experiments, including those requiring line-of-sight access to room temperature.

The modularity of the design ensures compatibility for upgrading existing cryogen-free dilution refrigerators, offering the opportunity for an order-of-magnitude decrease in their base temperature. To promote future sustainability and reduce the environmental impact, the manufacturing processes are designed to minimize the use of toxic and hazardous materials. The technological importance of $PrNi_5$ as a working material motivates the growth of samples of improved quality.

This work moves us from a *proof of principle* to a prototype system, with very limited demands on the surrounding infrastructure. The internal levels of vibration isolation achieved are sufficient to produce a low heat leak to the demagnetization stage, without massive support structures and optical-table-quality air mounts. As such, this is hopefully a significant step toward the accessibility of microkelvin temperatures, opening up a frontier in quantum information science and quantum material research to the widest possible community.

Acknowledgments.—We would like to thank Mark Meisel for useful discussions. The work in the London Low Temperature Laboratory was supported by the technical staff, in particular Richard Elsom, Ian Higgs, Paul Bamford, and Harpal Sandhu. The research leading to these results has received funding from the European Union Horizon 2020 research and innovation program, under Grant Agreement No. 824109.

[1] K. Uhlig, ^{3}He/^{4}He dilution refrigerator with pulse-tube refrigerator precooling, Cryogenics **42**, 73 (2002).
[2] G. Batey, *et al.*, Integration of superconducting magnets with cryogen-free dilution refrigerator systems, Cryogenics **49**, 727 (2009).
[3] https://emplatform.eu/.
[4] F. Pobell, *Matter and Methods at Low Temperatures* (Springer, Berlin, 2007), 1.
[5] S. E. de Graaf, *et al.*, Direct Identification of Dilute Surface Spins on Al_2O_3: Origin of Flux Noise in Quantum Circuits, Phys. Rev. Lett. **118**, 057703 (2017).
[6] S. E. de Graaf, *et al.*, Two-level systems in superconducting quantum devices due to trapped quasiparticles, Sci. Adv. **6**, eabc5055 (2020).
[7] P. Shor, in *Proceedings of 37th Conference on Foundations of Computer Science* (IEEE Computer Society, Los Alamitos, California, 1996), p. 56.
[8] C. Müller, J. H. Cole, and J. Lisenfeld, Towards understanding two-level-systems in amorphous solids: Insights from quantum circuits, Rep. Prog. Phys. **82**, 124501 (2019).
[9] N. Samkharadze, *et al.*, Integrated electronic transport and thermometry at millikelvin temperatures and in strong magnetic fields, Rev. Sci. Instrum. **82**, 053902 (2011).
[10] W. Pan, *et al.*, Exact Quantization of the Even-Denominator Fractional Quantum Hall State at $\nu = 5/2$ Landau Level Filling Factor, Phys. Rev. Lett. **83**, 3530 (1999).
[11] S.-C. Ho, *et al.*, Imaging the Zigzag Wigner Crystal in Confinement-Tunable Quantum Wires, Phys. Rev. Lett. **121**, 106801 (2018).
[12] M. Hays, *et al.*, Coherent manipulation of an Andreev spin qubit, Science **373**, 430 (2021).
[13] M. Sato and Y. Ando, Topological superconductors: A review, Rep. Prog. Phys. **80**, 076501 (2017).
[14] D. Shaffer, J. Kang, F. J. Burnell, and R. M. Fernandes, Crystalline nodal topological superconductivity and Bogolyubov Fermi surfaces in monolayer $NbSe_2$, Phys. Rev. B **101**, 224503 (2020).
[15] R. Sharma, *et al.*, Momentum-resolved superconducting energy gaps of Sr_2RuO_4 from quasiparticle interference imaging, Proc. Nat. Acad. Sci. **117**, 5222 (2020).
[16] A. K. Nayak, *et al.*, Evidence of topological boundary modes with topological nodal-point superconductivity, Nat. Phys. **17**, 1413 (2021).
[17] K. Nogaki, A. Daido, J. Ishizuka, and Y. Yanase, Topological crystalline superconductivity in locally noncentrosymmetric $CeRh_2As_2$, Phys. Rev. Res. **3**, L032071 (2021).
[18] S. Khim, *et al.*, Field-induced transition within the superconducting state of $CeRh_2As_2$, Science **373**, 1012 (2021).
[19] E. Schuberth, *et al.*, Emergence of superconductivity in the canonical heavy-electron metal $YbRh_2Si_2$, Science **351**, 485 (2016).
[20] T. Mizushima, *et al.*, Symmetry-protected topological superfluids and superconductors—From the basics to ^{3}He—, J. Phys. Soc. Jpn **85**, 022001 (2016).
[21] J. T. Mäkinen, *et al.*, Half-quantum vortices and walls bounded by strings in the polar-distorted phases of topological superfluid ^{3}He, Nat. Commun. **10**, 237 (2019).
[22] G. E. Volovik, ^{3}He universe 2020, J. Low Temp. Phys. **202**, 11 (2021).
[23] P. J. Heikkinen, *et al.*, Fragility of surface states in topological superfluid ^{3}He, Nat. Commun. **12**, 1574 (2021).
[24] S. Nakatsuji, *et al.*, Superconductivity and quantum criticality in the heavy-fermion system β-$YbAlB_4$, Nat. Phys. **4**, 603 (2008).
[25] W. T. Fuhrman, *et al.*, Pristine quantum criticality in a Kondo semimetal, Sci. Adv. **7**, eabf9134 (2021).
[26] S. Paschen and Q. Si, Quantum phases driven by strong correlations, Nat. Rev. Phys. **3**, 9 (2021).
[27] E. A. Chekhovich, *et al.*, Nuclear spin effects in semiconductor quantum dots, Nat. Mater. **12**, 494 (2013).

[28] P. Simon, B. Braunecker, and D. Loss, Magnetic ordering of nuclear spins in an interacting two-dimensional electron gas, Phys. Rev. B **77**, 045108 (2008).
[29] T. Kikkawa, *et al.*, Observation of nuclear-spin Seebeck effect, Nat. Commun. **12**, 4356 (2021).
[30] H. Eisenlohr and M. Vojta, Limits to magnetic quantum criticality from nuclear spins, Phys. Rev. B **103**, 064405 (2021).
[31] J. T. Muhonen, M. Meschke, and J. P. Pekola, Micrometre-scale refrigerators, Rep. Prog. Phys. **75**, 046501 (2012).
[32] J. P. Pekola and B. Karimi, Colloquium: Quantum heat transport in condensed matter systems, Rev. Mod. Phys. **93**, 041001 (2021).
[33] A. C. Clark, K. K. Schwarzwälder, T. Bandi, D. Maradan, and D. M. Zumbühl, Method for cooling nanostructures to microkelvin temperatures, Rev. Sci. Instrum. **81**, 103904 (2010).
[34] M. Palma, *et al.*, Magnetic cooling for microkelvin nanoelectronics on a cryofree platform, Rev. Sci. Instrum. **88**, 043902 (2017).
[35] A. T. Jones, *et al.*, Progress in cooling nanoelectronic devices to ultra-low temperatures, J. Low Temp. Phys. **201**, 772 (2020).
[36] M. Sarsby, N. Yurttagül, and A. Geresdi, 500 microkelvin nanoelectronics, Nat. Commun. **11**, 1492 (2020).
[37] L. V. Levitin, *et al.*, Cooling low-dimensional electron systems into the microkelvin regime, Nat. Commun. **13**, 667 (2022).
[38] J. Knapp, *et al.*, (unpublished).
[39] F. Bangma, *et al.*, (unpublished).
[40] G. Batey, *et al.*, A microkelvin cryogen-free experimental platform with integrated noise thermometry, New J. Phys. **15**, 113034 (2013).
[41] J. M. Parpia, *et al.*, Optimization procedure for the cooling of liquid ^{3}He by adiabatic demagnetization of praseodymium nickel, Rev. Sci. Instrum. **56**, 437 (1985).
[42] D. Schmoranzer, A. Luck, E. Collin, and A. Fefferman, Cryogenic broadband vibration measurement on a cryogen-free dilution refrigerator, Cryogenics **98**, 102 (2019).
[43] I. Todoshchenko, J.-P. Kaikkonen, R. Blaauwgeers, P. J. Hakonen, and A. Savin, Dry demagnetization cryostat for sub-millikelvin helium experiments: Refrigeration and thermometry, Rev. Sci. Instrum. **85**, 085106 (2014).
[44] J. Yan, *et al.*, Cryogen-free one hundred microkelvin refrigerator, Rev. Sci. Instrum. **92**, 025120 (2021).
[45] R. Toda, S. Murakawa, and H. Fukuyama, Design and expected performance of a compact and continuous nuclear demagnetization refrigerator for sub-mK applications, J. Phys.: Conf. Ser. **969**, 012093 (2018).
[46] D. Schmoranzer, *et al.*, Design evaluation of serial and parallel sub-mK continuous nuclear demagnetization refrigerators, Cryogenics **110**, 103119 (2020).
[47] K. Andres and S. Darack, Cooling of ^{3}He to 1 mK by nuclear demagnetization of $PrNi_5$, Phys. B+C **86-88**, 1071 (1977).
[48] R. Mueller, C. Buchal, H. Folle, M. Kubota, and F. Pobell, A double-stage nuclear demagnetization refrigerator, Cryogenics **20**, 395 (1980).
[49] H. R. Folle, M. Kubota, C. Buchal, R. M. Mueller, and F. Pobell, Nuclear refrigeration properties of $PrNi_5$, Z. für Phys. B Condens. Matter **41**, 223 (1981).
[50] D. S. Greywall, ^{3}He melting-curve thermometry at millikelvin temperatures, Phys. Rev. B **31**, 2675 (1985).
[51] S. Wiegers, *et al.*, Compact $PrNi_5$ nuclear demagnetization cryostat, Cryogenics **30**, 770 (1990).
[52] C. P. Lusher, *et al.*, Current sensing noise thermometry using a low T_c DC SQUID preamplifier, Meas. Sci. Technol. **12**, 1 (2000).
[53] A. Shibahara, *et al.*, Primary current-sensing noise thermometry in the millikelvin regime, Philos. Trans. R. Soc. A: Math., Phys. Eng. Sci. **374**, 20150054 (2016).
[54] Oxford Instruments NanoScience, UK. https://www.oxinst.com/.
[55] A. S. Rybalko and M. B. Sterin, Electrical and thermal conductivity of the conical thermal contacts used at ultra low temperature, Fiz. Nizk. Temp. **22**, 1095 (1996).
[56] Luvata Wolverhampton Ltd., UK. https://www.luvata.com/.
[57] Twickenham Plating Group, UK. http://twickenham.co.uk/.
[58] AMES Laboratory, U.S. Department of Energy, Iowa State University.
[59] M. Kubota, *et al.*, Nuclear Magnetic Ordering in $PrNi_5$ at 0.4 mK, Phys. Rev. Lett. **45**, 1812 (1980).
[60] J. Korringa, Nuclear magnetic relaxation and resonance line shift in metals, Physica **16**, 601 (1950).
[61] T. Herrmannsdörfer, H. Uniewski, and F. Pobell, Nuclear ferromagnetic ordering of ^{141}Pr in the diluted Van Vleck paramagnets $Pr_{1-x}Y_xNi_5$, J. Low Temp. Phys. **97**, 189 (1994).
[62] S. Takimoto, R. Toda, S. Murakawa, and H. Fukuyama, Construction of continuous magnetic cooling apparatus with zinc soldered $PrNi_5$ nuclear stages, J. Low Temp. Phys. **208**, 492 (2022).
[63] L. Lorenz, Determination of the degree of heat in absolute measure, Ann. Phys. **147**, 429 (1872).
[64] R. Franz and G. Wiedemann, Ueber die Wärme-Leitungsfähigkeit der Metalle, Ann. Phys. **165**, 497 (1853).
[65] J. Butterworth, *et al.*, Superconducting aluminum heat switch with 3 nΩ equivalent resistance, Rev. Sci. Instrum. **93**, 034901 (2022).
[66] R. W. Arenz, C. F. Clark, and W. N. Lawless, Thermal conductivity and electrical resistivity of copper in intense magnetic fields at low temperatures, Phys. Rev. B **26**, 2727 (1982).
[67] F. Fickett, Transverse magnetoresistance of oxygen-free copper, IEEE Trans. Magn. **24**, 1156 (1988).
[68] D. Drung, *et al.*, Highly sensitive and easy-to-use SQUID sensors, IEEE Trans. Appl. Supercond. **17**, 699 (2007).
[69] A. Casey, J. Saunders, L. Levitin, and H. van der Vliet, Current sensing noise thermometer (2021), Patent International Publication number: WO 2021/239513 A1.